Optical Fiber Technology 82 (2024) 103595

Contents lists available at ScienceDirect

Optical Fiber Technology

journal homepage: www.elsevier.com/locate/yofte

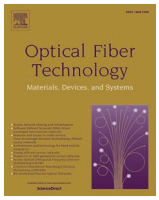

Regular Articles

Simplified colorless characterization scheme for coherent receivers in DWDM scenarios using a single interferer

P.J. Reyes-Iglesias [a,*], A. Ortega-Moñux [a], D. Izquierdo [b], I. Garcés [b], I. Molina-Fernández [a]

[a] Departamento Ingeniería de Comunicaciones, Telecommunication Research Institute (TELMA), Universidad de Málaga, CEI Andalucía TECH, 29071 Málaga, Spain
[b] Aragon Institute of Engineering Research (I3A), Universidad de Zaragoza, 50018 Zaragoza, Spain

ARTICLE INFO

Keywords:
Digital coherent receiver
Colorless operation
Filterless
Transparent optical network

ABSTRACT

Intradyne coherent receivers, capable of detecting an individual wavelength-division multiplexed channel just by tuning the local oscillator frequency, is of great interest for the development of high-capacity flexible optical networks. Nevertheless, the unavoidable amplitude imbalances inherent to any realistic coherent receiver induce an interference contribution from the self-beating of the coincident channels present at its input. The characterization of this degraded colorless reception operation is of fundamental importance, but it usually requires the use of rather complex experimental setups, especially when the effects of tens of interference channels should be evaluated. In this work we propose a novel experimental setup that only requires the use of a single intense interferer to emulate those coincident channels, thus drastically simplifying the characterization process. In addition, we develop a general expression for the signal-to-noise ratio of the system that theoretically justifies the intended setup and demonstrate by massive numerical simulations its accuracy in different scenarios. We believe that the proposed approach may contribute to facilitate the experimental characterization of high-performance colorless coherent receivers.

1. Introduction

The adoption of polarization multiplexing (PM) and efficient multi-level quadrature amplitude modulation (M−QAM) are extended solutions to increase bit rate capacity in fiber optic systems, beyond 100 Gbps, within the limited capabilities of electronic bandwidth and digital signal processing (DSP) [1,2]. A standard reception architecture is the conventional dual polarization (DP) balanced coherent receiver that relies on a polarization diversity network, based on polarization beam splitters (PBS), and two-phase diversity downconverters, based on 90° hybrids and balanced photodetection [2,3], for the demodulation of the in-phase and quadrature (IQ) components of each polarization. Besides its high chromatic and polarization mode dispersion tolerance, this digital coherent receiver can select and detect an individual dense wavelength-division multiplexed (DWDM) channel just by tuning the local oscillator (LO) frequency, being commonly known as filterless or colorless receivers [4–6]. This ability is of great interest in modern flexible optical networks deploying reconfigurable optical add-drop multiplexers (ROADM) which provide, from a remote control plane, the dynamic routing of any wavelength to a drop port [7,8]. Since a coherent receiver does not require any previous demultiplexer or WSS (wavelength selective switch), their partial replacement with optical splitters has led to the proposal of cost-effective drop node modules and simplified networks in WDM passive optical networks (PON) [9,10], intra-data center networks [7], as well as submarine [11] and terrestrial optical transport networks [12–14].

The photonic integration of the coherent receiver is of great interest in commercial applications due to its compactness, cost-effectiveness and low power consumption [15]. However, inevitable imbalances arising from fabrication tolerances, wideband operation or photodiodes responsivity will degrade the common-mode rejection ratio (CMRR) figure of the receiver. A high CMRR is required, not only to reject common output noise terms, as relative intensity noise (RIN) from LO, but to reduce the unwanted interference in baseband that arises from the self-beating of the coincident channels caused by the square-law of the photodetectors [5]. For this reason, it is important to determine how this limiting interference degrades the performance of a colorless receiver in terms of maximum number of channels that can be presented at its input as well as the resulting sensitivity and dynamic range parameters [4,5]. This characterization requires assembling a rather complex

* Corresponding author.
E-mail address: reyes@ic.uma.es (P.J. Reyes-Iglesias).

https://doi.org/10.1016/j.yofte.2023.103595
Received 1 August 2023; Received in revised form 27 October 2023; Accepted 9 November 2023
Available online 22 November 2023

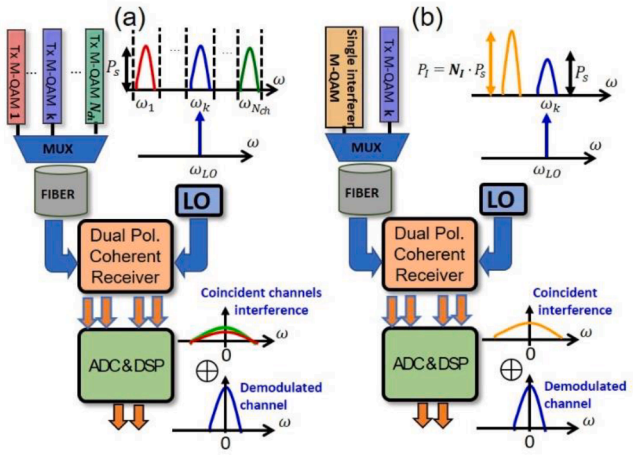

Fig. 1. Experimental setups to characterize the colorless performance of a DP coherent receiver: (a) conventional scheme: colorless reception under WMD coincident signals (b) simplified scheme proposed in this work: colorless reception of signal with a single interferer.

experimental setup that involves the transmission of tens of independent interfering channels, for instance, the evaluation of colorless reception of the full C-band under QPSK modulation could only be predicted from a limited set-up of 16 channels in [16] while it required eighty channels in [17]. In this work it is proposed a novel experimental scheme that significantly simplifies the characterization of the colorless operation of a coherent receiver as it only requires the use of a single interferer whose power scales accordingly to the number of coincident channels to be emulated. Additionally, a new simplified expression for the signal-to-noise ratio (SNR) of the system that justifies theoretically the intended setup, including the modulation format or symbol rate implications, is derived and verified from extensive numerical simulations. Its accuracy in different scenarios of practical receivers for incoming signals carrying up to 100 DWDM channels of 25 Gbaud DP-16/64QAM is analyzed. Without loss of generality, the procedure presented here could easily be applied to a higher baud rate, number of channels or QAM order, in line with the increasing demand on optical transceivers capacity.

This paper is organized as follows. In Section 2 the theory for characterizing the performance of colorless coherent receivers is presented both under multiple coincident WDM channels of the conventional scheme and under the single interference of our proposed scheme. The Appendix A provides a detailed derivation of the theoretical expressions. In Section 3, the coincidence between the theoretical prediction and the numerical model assessment is confirmed for both schemes in the colorless characterization of a coherent receiver with amplitude imbalances. Finally, Section 4 provides the main conclusions of this paper.

2. Conventional and proposed simplified experimental setup for the characterization of colorless receivers

In this section we describe the conventional setup commonly used to characterize the colorless operation of a coherent receiver under DWDM transmission (Fig. 1a) and the simplified approach proposed in this work (Fig. 1b). The main difference between these two schemes is clear in the figure: the conventional setup requires the simultaneous generation and subsequent combination of N_{ch} modulated signals with power P_s, whereas the new technique only requires the generation of a single and intense interference signal with a specific power level of value N_I times that of the signal channel P_s.

It can be theoretically shown (see Appendix A.1) that both schemes are characterized in terms of the SNR at the output of the receiver DSP block, involving state-of-the art algorithms, as

$$SNR = \frac{|S_{RX}|^2}{\sigma^2_{ASE\_LO} + k_{Imb}\left(CMRR^2 \cdot \left[\sigma^2_{RIN} + \sigma^2_{Interf}\right] + \sigma^2_{shot} + \sigma^2_{TIA}\right)} \tag{1}$$

where $\langle |S_{RX}|^2 \rangle$ is the demodulated average signal power, $\sigma^2_{ASE\_LO}$, σ^2_{RIN}, σ^2_{shot} and σ^2_{TIA} are respectively the noise current variance terms corresponding to LO beating with amplified spontaneous emission (ASE) noise, RIN from the LO laser, shot noise from the photodiodes and thermal-induced noise from the transimpedance amplifiers (TIA). The CMRR factor of the receiver is zero (in linear scale) for an ideal implementation, but it will increase with the amplitude imbalances of the receiver under test. Finally, the current variance of the interference caused by the adjacent or coincident channels results in the term σ^2_{Interf}. It is worth noting that the derived expression (1) is identical to that given in [4,18] except for the factor k_{Imb}, due to the excess power noise caused by Gram-Schmidt orthonormalization process (GSOP) at the DSP [19]. This factor improves the accuracy of the model and must be introduced to obtain a better fit between theoretical and numerical results.

As shown in Appendix A.1, the interference term from adjacent channels σ^2_{Interf} included in Eq. (1) is obviously different for each of the configurations shown in Fig. 1, since under uncorrelated equal power WDM channels (Fig. 1.a) the variance operator will respond from the sum of the variances proportionally to N_{ch}, while under a single interferer scaled to the signal by a factor N_I (Fig. 1.b) the variance will be proportional to its square. Thus, the interference term corresponds to

$$\sigma^2_{Interf} = \begin{cases} \frac{R^2}{2} \cdot P_s^2 \cdot N_{ch} \cdot \beta_{WDM} & \textit{Conventional scheme (Fig. 1a)} \\ \frac{R^2}{2} \cdot P_s^2 \cdot N_I^2 \cdot \beta_I & \textit{Simplified scheme proposed (Fig. 1b)} \end{cases} \tag{2}$$

where the corresponding scaling factors, β_{WDM} or β_I, are defined by the variance of the overlapped direct detection of the received channels obtained from their scheme in Fig. 1. Their value will strongly depend on the accumulated dispersion, baud rate, polarization alignment or QAM

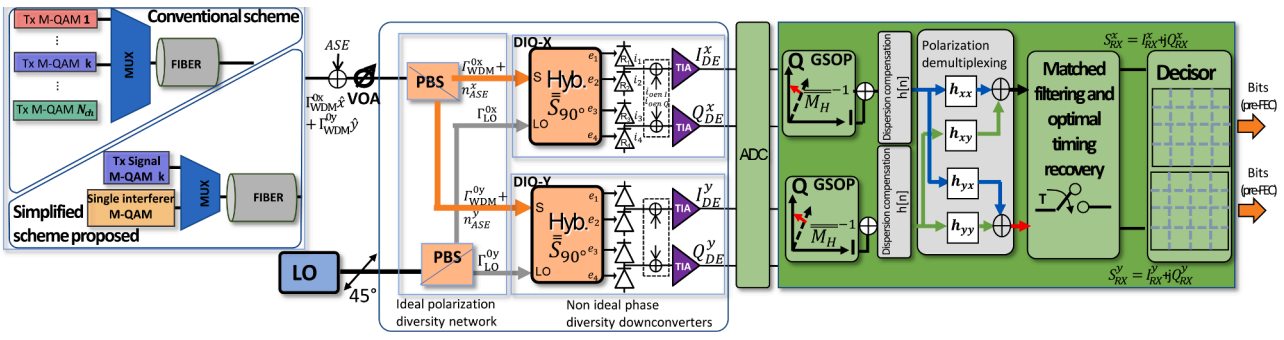

Fig. 2. Block diagram of the DP intradyne coherent receiver under test for the colorless demodulation of signal channel.

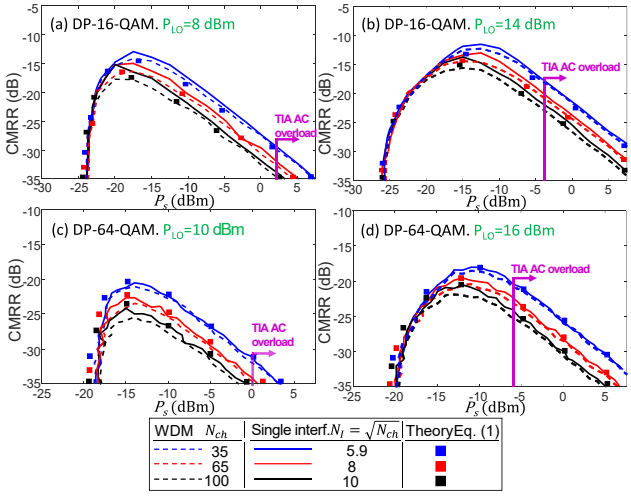

Fig. 3. Contour plot for a 1 dB Q-factor penalty of colorless coherent reception as a function of the CMRR and average input signal power (per polarization) under a single interferer (solid lines) for 25 Gbaud: DP-16-QAM (a) P_{LO} = 8 dBm (b) P_{LO} = 14 dBm; DP-64-QAM (c) P_{LO} = 10 dBm (d) P_{LO} = 16 dBm. The agreement with the theory (filled squares) and WDM transmission (dashed lines) is clearly appreciated when the relationship from the legend is fulfilled.

modulation order. A novel and detailed analysis, performed for the sake of clarity in Appendix A.2, shows that, when a minimum accumulated dispersion is reached in the fiber optic channel for a specific baud rate (according to Eq.(A.16)), both β_{WDM} and β_I will converge to a same value of 0.5 regardless of the modulation order. It is noteworthy that this scaling factor convergence value for both the conventional and simplified schemes coincide to a certain extent with previously reported experimental characterization under DP-QPSK modulation for balanced [4,16] and single-ended [18] coherent receivers, respectively. In fact, in [18] the use of a single interference channel, in a scheme that could be simplified to Fig. 1.b, was prematurely discarded as it was not properly scaled, even though the necessary polarization and time alignment independence between the interference and signal channels after high dispersive fiber propagation were experimentally confirmed. Certainly, by equating the interference terms in Eq. (2) under the above conditions, it can be obtained the simple relation $N_I = \sqrt{N_{ch}}$ that results on a same SNR and supports our experimental proposal from Fig. 1 to emulate the colorless performance of a receiver with N_{ch} coincident channels of power P_s from a single interference of power N_I times greater,

$$P_I = N_I \cdot P_s = \sqrt{N_{ch}} \cdot P_s \tag{3}$$

We would like to emphasize that, although equation (3) may seem a straightforward result, this is only fulfilled if both scaling factors β_{WDM} and β_I present the same value which occurs when the accumulated dispersion of the fiber preceding the receiver exceeds the minimum value from Eq.(A.16). Specifically, for the 25 Gbaud symbol rate adopted in this work, the minimum accumulated dispersion results in 2 ns/nm, as graphically depicted in Fig. 6 of Appendix A.2.

3. Colorless coherent reception model assessment

This section is divided into two parts. The first part shows the modelling of the coherent receiver under test. In the second part, a complete set of numerical simulations is performed to confirm the accuracy of the expressions shown for both schemes in the previous section and, consequently, the feasibility of the proposed technique.

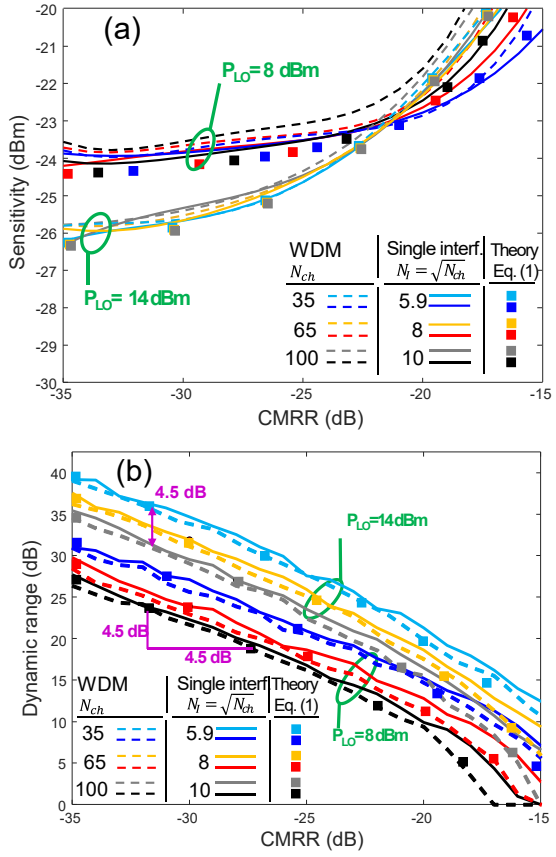

Fig. 4. Sensitivity (a) and dynamic range (b) as a function of CMRR for the colorless reception under a single interferer (solid lines) for 25 Gbaud DP-16-QAM modulation showing clear coincidence with colorless reception under WDM transmission (dashed lines) and theory (filled squares) when the relationship from the legend is fulfilled.

3.1. Colorless coherent receiver simulation environment

According to the usual setup scheme from Fig. 1.a, a WDM signal, obtained by combining N_{ch} channels under DP-M−QAM modulation, will be transmitted into a dispersive single-mode fiber modelled using Jones matrix formalism with random mode coupling (RMC) and additive white Gaussian noise (AWGN) to account for ASE noise from optical amplifiers. To statistically emulate the independence of a multi-channel transmission, different seeds were considered to generate pseudo-random binary sequences (PRBS), arbitrary time delays and random polarization orientations for each channel. Incoming optical signal-to-noise ratio (OSNR) has been adjusted for the incident signal channels to obtain a BER of 7×10^{-4} in an ideal coherent receiver in absence of internal noise sources The input signal power level was then controlled by a variable optical attenuator (VOA). In the proposed setup scheme from Fig. 1.b, there will be a unique interference with power N_I times greater than signal according to Eq. (3).

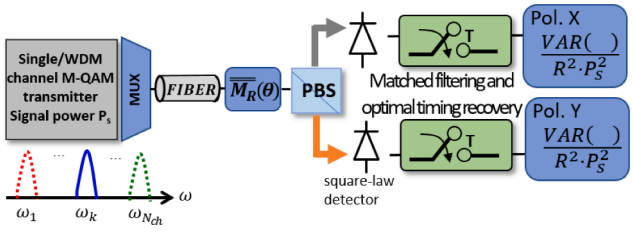

Fig. 5. Scheme for the numerical estimation of the scaling factors.

In both schemes it will be induced an accumulated chromatic dispersion of 2 ns/nm, e.g. obtained from the transmission in the third optical window through 125 km of standard single-mode fiber (SSMF), above which the scaling factors β_{WDM} and β_I of Eq. (2) have already converged to a same value of 0.5 for the adopted symbol rate of 25 Gbaud, as determined by Eq. (A.16). The maximum allowable accumulated dispersion, and hence the maximum length of the fiber prior the receiver, will only be limited by the availability of a sufficient number of taps in the finite-impulse-response (FIR) filters required to compensate for the induced dispersion in the DSP from the demodulated signal [20].

Fig. 2 describes in more detail the conventional DP intradyne coherent receiver under test for the colorless demodulation of a k^{th} channel using a LO laser tuned to the adequate wavelength, with power P_{LO} and a RIN value of −140 dB/Hz. The polarization diversity network consists of two PBS in both the signal and LO paths [4,21,22]. The phase diversity downconverters are based on 90° optical hybrids followed by two balanced photodiodes (BPD) with mean responsivity 0.8 A/W and TIAs with DC offset cancellation and an input referred thermal noise current density of $\alpha_{TIA}^2 = 20\ pA/\sqrt{Hz}$. The obtained IQ components per polarization of the downconverted signal channel will be then digitized by four analog-to-digital converters (ADC) with the minimum effective number of bits (ENOB) to induce a negligible penalty (6 bits for 16-QAM and 7 bits for 64-QAM [23]) and combined to be further processed in the DSP. Phase diversity imbalances, contributing to CMRR values ranging from −35 dB to −5 dB ($CMRR\ [dB] = 20{\cdot}log_{10}\ (CMRR)$), will induce a linear transformation of the IQ components, resolved by a GSOP procedure [19], and a detrimental nonlinear interference by the self-beating of the adjacent channels [5]. The polarization demultiplexing will be then performed by a 2 × 2 butterfly configuration FIR filter being followed by a matched filter presenting optimal timing recovery to provide numerical results comparable to the theoretical expressions. Error counting is evaluated after the decisor to calculate the bit-error-rate (BER). Finally, the receiver performance will be then quantified by the Q-factor (an average from the *x/y* polarization) assuming Gaussian distribution of overall noise sources [4,20],

$$Q\ (dB) = 20{\cdot}\log\left[\sqrt{2}\cdot erfc^{-1}(2{\cdot}BER)\right] \tag{4}$$

where *erfc* is the complementary error function.

On the other hand, as a comparison, the theoretical Q-factor will be obtained from the theoretical estimation of the BER for a homodyne receiver determined by the analytical SNR in Eq. (1) assuming M-QAM modulation [23,24]

$$BER = \frac{1}{\log_2 M}\left\{1 - \left[1 - \left(1 - \frac{1}{\sqrt{M}}\right) erfc\left(\sqrt{\frac{3}{2(M-1)}SNR}\right)\right]^2\right\}. \tag{5}$$

In both numerical and theoretical cases, a maximum admissible Q-factor penalty of 1 dB will be considered, which will ensure a BER below the limit of 2.2×10^{-3} for a typical forward error correction (FEC) coding with 7 % redundancy overhead [25].

3.2. Simulation results of colorless coherent reception of signal channel under coincident WDM channels and a single interferer

Theoretical expressions Eq. (1)–(3) characterizing the colorless reception scenarios depicted in Fig. 2 will be validated here carrying out extensive numerical simulations for DP-16-QAM and DP-64-QAM signals and for some representative LO powers. Fig. 3 shows the contour plot for 1 dB Q-factor penalty as a function of the CMRR and input signal power for the colorless reception of a signal coincident with a single interferer (solid lines) and from N_{ch} WDM channels (dashed lines) accordingly to the proposed (Fig. 1.b) and conventional (Fig. 1.a) schemes, respectively. Legend shows the relationship that, accordingly

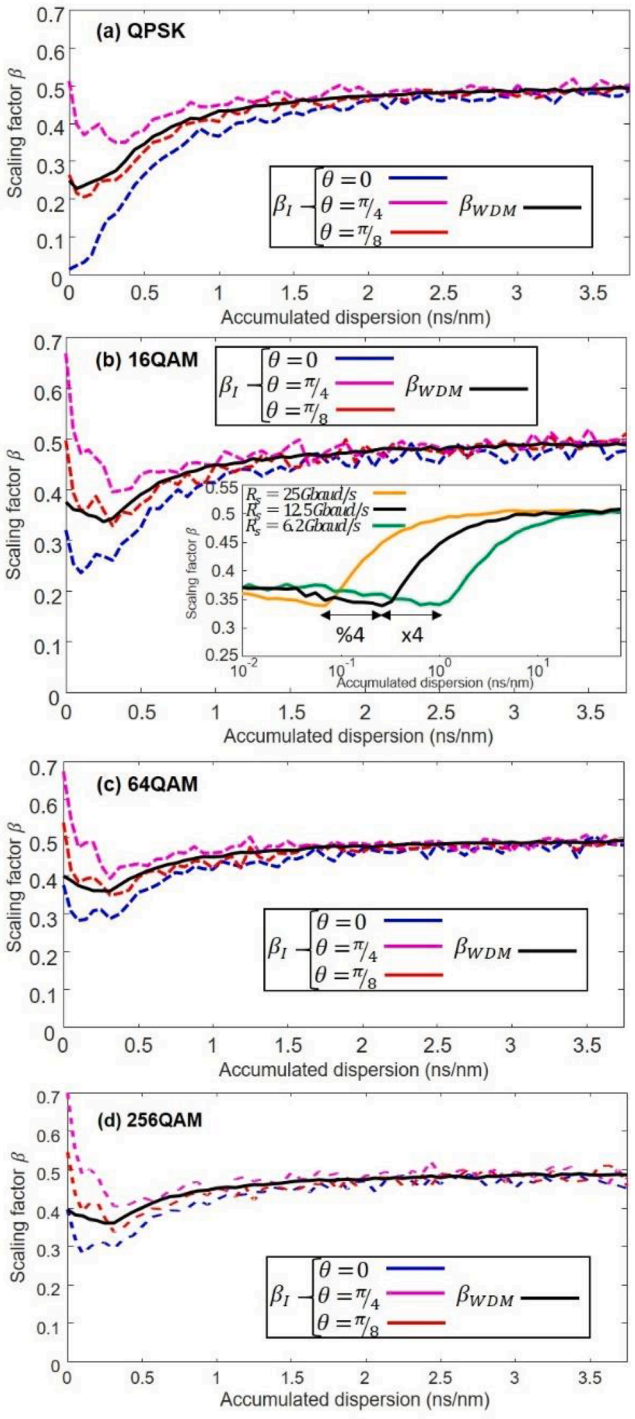

Fig. 6. Numerical estimation of scaling factors β_I and β_{WDM} versus the accumulated dispersion for different orders of QAM modulation at 25 Gbaud: (a) QPSK (b) 16-QAM (inset represents the β_{WDM} dependence with the symbol rate) (c) 64-QAM (d) 256-QAM.

to Eq. (3), N_I meets for a specific N_{ch} value for a correct emulation. Note that the area under each curve from Fig. 3 defines a valid transmission zone where the BER of the demodulated signal will be below FEC limit. It can be clearly appreciated the good agreement between the numerical results of the analyzed schemes and with theoretical prediction superimposed as a reference (filled squares). Therefore, it is shown that characterization of practical colorless coherent receivers can be achieved from the setup proposed in Fig. 1.b that greatly simplifies the conventional scheme depicted in Fig. 1.a.

Each of the 1 dB penalty contour curves in Fig. 3 presents two cut-off points for the specific CMRR value of the receiver. The first one (lower signal power) determines the sensitivity and its difference with the second one (higher signal power), the dynamic range. At the low signal power regime, the receiver sensitivity worsens from the shot-noise limit performance when the CMRR degrades as the residual LO-RIN beat noise will dominate for high LO power. In the high signal power regime, it can be easily appreciated the significant reduction of the dynamic range as N_I (or equivalently N_{ch}) increases and the CMRR deteriorates due to the enhanced interference term σ^2_{Interf} caused by the self-beating of the coincident channels. The incidence of the interfering term in the demodulated signal under the above considerations will only be reduced by increasing the LO power as long as we assure TIA linear operation. Certainly, the maximum allowable nonlinear harmonic distortion from TIAs will limit the maximum differential AC input current. For instance, considering a dispersion-induced peak-to-average (PAPR) power ratio of 10 dB in the demodulated signal [4,16] and a typical AC input overload current of 4 mApp [26], the maximum signal power would be limited by the magenta lines plotted in Fig. 3. Finally, it is noteworthy the habitual integration of VOA in the signal path of the colorless coherent receiver for the optimal use of available dynamic range [3,27].

A better insight of the degradation induced by amplitude imbalances (quantified by the CMRR) in the sensitivity and dynamic range of a colorless receiver can be observed in Fig. 4.a and Fig. 4.b, respectively, according to the results obtained for the DP-16-QAM signals from Fig. 3. Here, a clear coincidence between the obtained numerical curves for the proposed scheme (solid lines), the conventional scheme (dashed lines) and the theoretical prediction (superimposed filled squares) can be also appreciated when Eq. (3) is fulfilled. As it can be seen from the sensitivity evolution in Fig. 4.a for a high CMRR (above 25 dB in absolute value), shot-noise limit performance will be achieved increasing the LO power. In addition, as shown in Fig. 4.b, the residual interference from coincident channels (see Eq. (1)–(2)) will decrease the signal dynamic range on a logarithmic scale with the CMRR deterioration (e.g. the dynamic range shows a 4.5 dB reduction when the CMRR worsens by 4.5 dB, regardless of LO and N_{ch} values) and the number of channels (e.g., a reduction of 4.5 dB when N_{ch} is increased by 4.5 dB or from 35 to 100 channels). On the other hand, the deterioration of the CMRR (approximately under 25 dB in absolute value) will increase the residual RIN from the LO, reducing the sensitivity in Fig. 4.a and, consequently, the dynamic range as can be seen from the increase of its corresponding slope in Fig. 4.b.

It can be stated from Fig. 3 and Fig. 4 that, if we want to achieve a large dynamic range under colorless reception of DWDM DP-M-QAM signals, the higher the modulation order M, the stricter control of receiver amplitude imbalances for a fixed LO power will be required to assure a high CMRR in the operation band. Therefore, it follows that the minimum value of 20 dB specified by the OIF as an adequate CMRR for an intradyne coherent receiver [3] is barely enough for practical colorless reception of higher-order modulation.

4. Conclusions

The availability of colorless intradyne coherent receivers is of great interest for the development of high-capacity flexible optical networks. However, unavoidable receiver amplitude imbalances will degrade its colorless operation due to the limiting baseband interference induced by the self-beating of coincident channels presented at its input. In this work we have proposed a novel experimental setup that drastically simplifies the colorless characterization of coherent receivers.

Unlike the conventional approach, based on a complex and expensive experimental setup involving the simultaneous transmission of tens of interference channels, the new approach only requires the injection of a single intense interferer of a specific power level, which scales with the square root of the number of interference channels to be emulated. The proposed scheme has first been theoretically justified using a simplified expression for the system SNR (derived in the Appendix A), and then accurately verified from extensive numerical simulations in different scenarios (up to 100 interference channels with DP-QAM modulation). Moreover, using these simulations we have been able to analyze the colorless behaviour of intradyne coherent receivers in terms of sensitivity and dynamic range variation as a function of the CMRR characteristics of the device. In the authors' opinion, the simplified scheme proposed in this work will contribute to facilitate the experimental characterization of high performance colorless coherent receivers, reducing the complexity and cost of the required experimental setup.

CRediT authorship contribution statement

P.J. Reyes-Iglesias: Conceptualization, Software, Investigation, Writing – original draft. **A. Ortega-Moñux:** Methodology, Writing – review & editing. **D. Izquierdo:** Writing – review & editing. **I. Garcés:** Writing – review & editing. **I. Molina-Fernández:** Supervision.

Declaration of Competing Interest

The authors declare that they have no known competing financial interests or personal relationships that could have appeared to influence the work reported in this paper.

Data availability

The data that has been used is confidential.

Acknowledgements

This work was supported in part by funds provided by Ministerio de Economía y Competitividad PID2019-106747RB-I00, Project TED2021-130400B-I00/ AEI/10.13039/501100011033/ Unión Europea Next-Generation EU/PRTR and Ministerio de Ciencia e Innovación - Agencia Estatal de Investigación PID2020-114916RB-I00. Funding for open access charge: Universidad de Málaga / CBUA.

Appendix A

For the sake of simplicity, it is detailed here the derived analytical expressions for the SNR of an imbalanced colorless coherent receiver and its interference term under WDM and single interferer reception schemes.

A.1 SNR of an imbalanced colorless coherent receiver for WDM transmission and a single interferer

This appendix evaluates the SNR of the demodulated channel in a non-ideal colorless coherent receiver following the block diagram model in Fig. 2. The results obtained for N_{ch} WDM channels with negligible crosstalk, following the conventional scheme from Fig. 1.a, will be easily particularized afterwards to a signal coincident with a single interference, according to the proposed scheme from Fig. 1.b.

The transmitted WDM optical signal will be described in terms of its complex envelope as (omitting for clarity the superscript *x/y* corresponding to each polarization)

$$\Gamma^{O}_{WDM} = \sum_{n=1}^{N_{ch}} \sqrt{P_{sn}} \cdot \Gamma_n \cdot e^{j\omega_n t} \tag{A.1}$$

where for each n^{th} channel, ω_n is the angular frequency, P_{sn} is the power and $\Gamma_n = \mathrm{I}_n + j\mathrm{Q}_n$ is the normalized complex baseband transmitted symbols satisfying $\langle |\Gamma_n|^2 \rangle = 1$ (where $\langle\,\rangle$ denotes the ensemble average operator). It will be considered a basic AWGN channel model, since the dispersive effects can be efficiently compensated in the subsequent DSP, accounting the contribution of complex ASE noise from n_{ASE} with power P_{ASE} in the receiver equivalent noise bandwidth B_e.

The polarization diversity network in the receiver consists of two PBS in both the signal and LO paths [4,21]. For homodyne detection of the k^{th} channel, the LO must be tuned to the angular frequency ω_k, being its complex envelope per polarization component at the exit of the PBS (also omitting here the superscripts *x/y*),

$$\Gamma^{O}_{LO} = \sqrt{\frac{P_{LO}}{2}} e^{j\omega_k t}. \tag{A.2}$$

On the following the superscripts *x/y* will be omitted, thus considering the same response for both phase diversity downconverters. In this way, the colorless detection of the k^{th} channel of the WDM signal Eq. (A.1) using the frequency-tuned LO Eq. (A.2) will result in each of the following four photocurrents i_i^k at the photodiodes after the 90° hybrid, considering a square-law photodetection and responsivity R_i,

$$i_i^k = R_i \left| e_i^k \right|^2 = R_i \left| \sum_{n=1}^{N_{ch}} S^n_{i\ S} \left(\sqrt{P_{sn}}\, \Gamma_n e^{j\omega_n t} + n_{ASE\ n} \right) + S^k_{i\ LO} \Gamma^0_{LO} \right|^2 ; i = 1,2,3,4 \tag{A.3}$$

where 90° hybrids are characterized at a frequency ω_n from the following scattering matrix $\overline{\overline{S}}_{90^\circ}$,

$$\overline{\overline{S}}_{90^\circ}(\omega_n) = \begin{bmatrix} S^n_{1\ S} & S^n_{1\ LO} \\ S^n_{2\ S} & S^n_{2\ LO} \\ S^n_{3\ S} & S^n_{3\ LO} \\ S^n_{4\ S} & S^n_{4\ LO} \end{bmatrix} \tag{A.4}$$

Note that an ideal 90° hybrid will have within the operation band the scattering parameters $\{S^n_{1\ S} = S^n_{2\ S} = S^n_{3\ S} = S^n_{4\ S} = 1/2,\ S^n_{1\ LO} = -S^n_{2\ LO} = 1/2,\ S^n_{3\ LO} = -S^n_{4\ LO} = j/2\}$

The introduction of uncorrelated optoelectronic AWGN noise sources, i_{oen_I} and i_{oen_Q} (including shot noise and thermal noise from TIA amplification), and the balanced photodetection will allow to solve the IQ components $\Gamma_{DE} = \mathrm{I}_{DE} + j\mathrm{Q}_{DE}$ of the downconverted k^{th} channel at the input of the DSP (neglecting high frequency beating terms which will be filtered out by the electronics),

$$\begin{bmatrix} I_{DE} \\ Q_{DE} \end{bmatrix} = \begin{bmatrix} i_1^k - i_2^k \\ i_3^k - i_4^k \end{bmatrix} = \sqrt{\frac{P_{OL}}{2}} \overline{\overline{M}}_H \cdot \begin{bmatrix} R_I \cdot Re\left(\sqrt{P_{sk}}\, \Gamma_k + n_{ASE\ k} \right) \\ R_Q \cdot Im\left(\sqrt{P_{sk}}\, \Gamma_k + n_{ASE\ k} \right) \end{bmatrix} + \frac{P_{LO}}{4} \begin{bmatrix} R_I \cdot CMRR^k_{LO\ I} \\ R_Q \cdot CMRR^k_{LO\ Q} \end{bmatrix} +$$

$$\frac{1}{2} \sum_{n=1}^{N_{ch}} \begin{bmatrix} R_I \cdot CMRR^n_{S\ I} \\ R_Q \cdot CMRR^n_{S\ Q} \end{bmatrix} \left(P_{sn} |\Gamma_n|^2 + 2Re\left(\sqrt{P_s}\, \Gamma_n \cdot n^*_{ASE\ n} \right) \right) + \begin{bmatrix} i_{oen\_I} \\ i_{oen\_Q} \end{bmatrix} \tag{A.5}$$

where it has been defined an average BPD responsivity $R_I = (R_1 + R_2)/2$ and $R_Q = (R_3 + R_4)/2$. Equation (A.5) has been expressed in terms of the CMRR (in linear scale), typical figure of merit of the colorless behaviour of a downconverter [3,5] since it is a direct measurement of its power imbalance at the frequency ω_k,

$$CMRR^n_{\substack{S\ I \\ LO\ I}} = \frac{\gamma^n_{1\ S\ 1\ LO} - \gamma^n_{2\ S\ 2\ LO}}{\gamma^n_{1\ S\ 1\ LO} + \gamma^n_{2\ S\ 2\ LO}};\ CMRR^n_{\substack{S\ Q \\ LO\ Q}} = \frac{\gamma^n_{3\ S\ 3\ LO} - \gamma^n_{4\ S\ 4\ LO}}{\gamma^n_{3\ S\ 3\ LO} + \gamma^n_{3\ S\ 4\ LO}} \tag{A.6}$$

where it has been described the intensity response in each output port with respect to the S / LO input port from,

$$\gamma^{n}_{\substack{i\ S\\ i\ LO}} = R_i \left| S^{n}_{\substack{i\ S\\ i\ LO}} \right|^2 ;\ i = 1\ldots4 \tag{A.7}$$

The phase diversity downconverter has been described by the complex matrix $\overline{\overline{M}}_H$,

$$\overline{\overline{M}}_H = \begin{bmatrix} Re(u) & Im(u) \\ Re(v) & Im(v) \end{bmatrix};\ \begin{matrix} u = \left(R_1 S^{k}_{1LO} S^{k*}_{1S} - R_2 S^{k}_{2LO} S^{k*}_{2S}\right)/(R_1 + R_2) \\ v = \left(R_3 S^{k}_{3LO} S^{k*}_{3S} - R_4 S^{k}_{4LO} S^{k*}_{4S}\right)/(R_3 + R_4) \end{matrix} . \tag{A.8}$$

It can be easily observed that for an ideal receiver implementation (CMRR = 0, same responsivity on the photodiodes and unitary matrix $\overline{\overline{M}}_H$), the demodulated IQ components in the first term on the right side of Eq. (A.5) will be only limited by the ASE noise (once defined the OSNR at the input receiver) and the receiver optoelectronic noise sources in the last term as it has been extensively studied [24,28]. This confirms the superior performance of balance detection over single-ended detection in this scenario. The second and third terms define the relative LO intensity noise (RIN noise) and the baseband interference caused by the adjacent channels from their self and noise beating (this latter can be considered negligible for the higher order M−QAM modulations considered in this paper), respectively. Note that the limiting self-beating interference term from the adjacent channels, uncorrelated with the demodulated IQ signal components, will be weighted by their signal power, number and the CMRR at their respective wavelengths [5].

Next, it will be considered non-ideal 90° hybrids with scattering matrix $\overline{\overline{S}}_{90^\circ}$ in the operation band,

$$\overline{\overline{S}}_{90^\circ} = \frac{1}{2}\begin{bmatrix} 1 & 1 \\ I_{mbI} & -I_{mbI} \\ 1 & \mathrm{j}e^{j\varnothing_{PE}} \\ I_{mbQ} & -\mathrm{j}I_{mbQ}e^{j\varnothing_{PE}} \end{bmatrix} \tag{A.9}$$

defined in terms of the amplitude imbalance factor (I_{mbI}, I_{mbQ}) and phase error ϕ_{PE} between IQ axes. It is reduced to ideal scattering matrix when $I_{mbI} = I_{mbQ} = 1$ and $\phi_{PE} = 0^\circ$. Being obtained from Eq. (A.6)–(A.7) the following CMRR from the input S/LO ports to I/Q component signal outputs,

$$CMRR^{n}_{\substack{S\\ LO\ I}\ \ I} = CMRR_I = \frac{R_1 - R_2 I^2_{mbI}}{R_1 + R_2 I^2_{mbI}};\ CMRR^{n}_{\substack{S\\ LO\ Q}\ \ Q} = CMRR_Q = \frac{R_3 - R_4 I^2_{mbQ}}{R_3 + R_4 I^2_{mbQ}} \tag{A.10}$$

and, solving Eq. (A.8), the downconverter transformation matrix $\overline{\overline{M}}_H$., represented here as the product of two matrices responsible of the imbalance and rotation between reference IQ axes to account for amplitude and phase imbalances, respectively,

$$\overline{\overline{M}}_H = \begin{bmatrix} \dfrac{R_1 + R_2 I^2_{mbI}}{2R_I} & 0 \\ 0 & \dfrac{R_3 + R_4 I^2_{mbQ}}{2R_Q} \end{bmatrix} \begin{bmatrix} 1 & 0 \\ -sin\varnothing_{PE} & \cos\varnothing_{PE} \end{bmatrix} \tag{A.11}$$

Particularizing Eq. (A.11) when considering a unique CMRR for the IQ signal components ($CMRR = CMRR_I = CMRR_Q$) and a same average BPD responsivity ($R = R_I = R_Q$), it will be solved the following expression for the demodulated signal at the output of the DSP $S_{RX} = I_{RX} + jQ_{RX}$.

$$\begin{bmatrix} I_{RX} \\ Q_{RX} \end{bmatrix} = R\sqrt{\frac{P_{LO}}{2}} \begin{bmatrix} Re\left(\sqrt{P_s}\Gamma_k + n_{ASE\ k}\right) \\ Im\left(\sqrt{P_s}\Gamma_k + n_{ASE\ k}\right) \end{bmatrix} + \overline{\overline{M}}_H^{-1} \left\{ R\frac{P_{LO}}{4} CMRR \begin{bmatrix} 1 \\ 1 \end{bmatrix} + \frac{R}{2} CMRR \begin{bmatrix} 1 \\ 1 \end{bmatrix} \sum_{n=1}^{N_{ch}} \left(P_{sn}|\Gamma_n|^2\right) + \begin{bmatrix} i_{oen\_I} \\ i_{oen\_Q} \end{bmatrix} \right\} \tag{A.12}$$

Note that the digital GSOP procedure performs the inverse of the downconverter matrix $\overline{\overline{M}}_H$, correcting phase/amplitude imbalances in the demodulated IQ signal but transforming the seconterm that accounts for the noise-interference generated. As it was studied in [22] for a non-ideal polarization diversity network, the Frobenius norm of transformation matrix $\overline{\overline{M}}_H^{-1}$ would estimate an excess power noise factor k_{Imb},

$$k_{Imb} = \frac{\overline{\overline{M}}^{-12}_{HF}}{\overline{\overline{M}}^{-12}_{HidealF}} = R^2 \left[\left(\frac{1 + CMRR}{R_1} \right)^2 \right] \sec^2\varnothing_{PE}. \tag{A.13}$$

It can be easily verified than an ideal downconverter (CMRR = 0, phase error $\phi_{PE} = 0^\circ$ and same responsivity) will have an identity matrix $\overline{\overline{M}}_H$ and, therefore, will not induce any sensitivity penalty k_{Imb} [dB] = 10· $\log_{10}$ (k_{Imb}) as $k_{Imb} = 1$. As phase errors of up to 20° (much higher than the 7.5° specified by the OIF in the operation band [3]) induce from Eq. (A.13) a sensitivity penalty of only 0.5 dB, from now on, it will only be considered the amplitude imbalances (quantified from the CMRR) to address the nonideality of the phase diversity downconverter.

At this point it can be solved the signal to noise and interference power ratio after the DSP (henceforth SNR),

$$SNR = \frac{|S_{RX}|^2}{\sigma^2_{ASE\_LO} + k_{Imb}\left(CMRR^2 \cdot \left[\sigma^2_{RIN} + \sigma^2_{Interf}\right] + \sigma^2_{shot} + \sigma^2_{TIA}\right)} \tag{A.14}$$

Note that we could have obtained the same SNR for each signal component and polarization as it was assumed that the CMRR was constant for them. The numerator corresponds to the demodulated average signal power $\langle|S_{RX}|^2\rangle = R^2 P_s P_{LO}/2$. The terms in the denominator accounts for the noise current variance values of the noise and interference terms: beating LO-ASE noise $\sigma^2_{ASE\_LO}$, relative intensity noise from LO σ^2_{RIN}, interference from adjacent channels σ^2_{Interf}, shot noise σ^2_{shot} and thermal-induced TIA noise σ^2_{TIA}. The expression that describes each one can be easily deduced [24] as

$$\sigma^2_{ASE\_OL} = R^2 P_{ASE}\frac{P_{LO}}{2};\ \sigma^2_{RIN} = \frac{R^2}{8} RIN \cdot B_e \cdot P^2_{LO}$$

$$\sigma^2_{shot} = qB_e R P_{LO};\ \sigma^2_{TIA} = 2\cdot\alpha^2_{TIA} B_e \tag{A.15}$$

$$\sigma^2_{Interf} = \begin{cases} \frac{R^2}{2}\cdot P_s^2 \cdot N_{ch} \cdot \beta_{WDM};\ \beta_{WDM} = \frac{1}{N_{ch}} VAR\left(\sum_{n=1}^{N_{ch}} |\Gamma_n|^2\right) & \text{Conventional scheme Fig.1a} \\ \frac{R^2}{2}\cdot P_s^2 \cdot N_I^2 \cdot \beta_I;\quad \beta_I = VAR\left(|\Gamma_I|^2\right) & \text{Simplified scheme proposed Fig. 1b} \end{cases}$$

In Eq. (A.14), which bears a similarity with those shown in [4,18], it will have great importance the interference term σ^2_{Interf} defined by the variance (denoted by the VAR operator) of the overlapped direct-detected channels. Under uncorrelated WDM channels of a same power P_s, corresponding to the conventional setup from Fig. 1.a, this term will be proportional in N_{ch} times a scale factor β_{WDM} defined by the average variance of the direct detection of the received normalized symbols. On the other hand, for the proposed scheme from Fig. 1.b, the interference will be practically imposed by the variance of the direct detection of the intense interferer with power $N_I \cdot P_s$. Note that this interference term can be seen as a particular case of the previous one where N_I channels are coherently added so that the variance will depend on the square of N_I. As it was already stated in [18], the number of channels N_{ch} is not directly extrapolated here to N_I nor, in principle, the values of the coefficients β_{WDM} equivalent to β_I. The detailed study of these scaling factors will be assessed in the following appendix subsection.

A.2 Numerical estimation of the scaling factor of the interference term

Fig. 5 shows the scheme adopted for the numerical estimation of the variance of the overlapped direct-detected channels as defined from the scaling factors β_{WDM} and β_I from Eq. (A.15). There it will be adjusted the order of QAM modulation, the accumulated dispersion and the control, through a Jones rotation matrix $\overline{\overline{M_R}}(\theta)$, of the input orientation. This is so because, as observed in [4,16,18], the scaling factor of the interfering channel will depend on its incidence orientation angle θ with respect the PBS receiver axes and the PAPR induced from the conversion of phase into intensity variations by the accumulated dispersion. Numerical simulations have been carried out from 20 frames of 4096 symbols of DP-M−QAM signal and a single-mode fiber link with an accumulated dispersion up to 3.8 ns/nm. The matched filter and normalization of the photodiode power readings will allow to assess the scaling factor β_I for a single interference or β_{WDM} for a WDM signal transmission (representative averaging from just 25 channels with random alignment times).

Fig. 6 shows in solid and dashed line the numerical estimation of the scaling factor β_{WDM} and β_I (as a function of the incidence angle θ), respectively, versus the accumulated dispersion for different orders of QAM modulation, M, at 25 Gbaud, thus expanding the study carried out for QPSK at 11.5 Gbaud and 28 Gbaud in [18] and [16], respectively. It is observed that the scaling factor β_I for a single interferer is minimized when its independent polarization components do not beat as are aligned with each PBS axis ($\theta = 0°$), being obtained a result equivalent to a back-to-back transmission and described analytically by $\beta_I = 2\cdot(M-4)/5\cdot(M-1)$. Conversely, the factor β_I will be maximized for $\theta = 45°$ from the beating of one-half power of each polarization components received on each PBS axis. The evolution of the scaling factor β_I for $\theta = 22.5°$ is similar to the factor β_{WDM}. In any case, as expected, the scaling factors β_I and β_{WDM} will grow with the accumulated dispersion until reaching a maximum of 0.5, independently of the time alignment or orientation respect the PBS receiver axes, when the PAPR does not increase further, which happens at a symbol rate of 25 Gbaud above 2 ns/nm. This last value is inversely proportional to the square of the symbol rate R_s. Thus, as the inset of Fig. 6.b represents for β_{WDM} under 16-QAM, that value will correspond to 8 ns/nm for half its symbol rate $R_s = 12.5$ Gbaud, as it was certainly obtained for QPSK in [4,18].

Therefore, the numerical results shown in Fig. 6 allow us to identify a scenario of interest as both scaling factors β_I and β_{WDM} converge to a same value of 0.5, independently of the QAM modulation order, when the accumulated dispersion AD [ns/nm] at the receiver input reach a minimum value that, according to the inset from Fig. 6.b for a symbol rate R_s in [Gbaud], is:

$$AD_{\min}\left[\frac{ns}{nm}\right] = 2\cdot\left(\frac{25}{R_s}\right)^2 \tag{A.16}$$

The minimum accumulated dispersion of 2 ns/nm, corresponding to the 25 Gbaud symbol rate considered in this work, could be obtained in the third transmission window (centered at 1550 nm) with a minimum standard single-mode fiber length of 125 km, since it has a dispersion coefficient of 16 ps/(nm·km).

References

[1] Optical Internetworking Forum, "Flex Coherent DWDM Transmission Framework Document," [Online] https://www.oiforum.com/technical-work/implementation-agreements-ias/.

[2] Optical Internetworking Forum, "Technology Options for 400G Implementation," [Online] https://www.oiforum.com/technical-work/implementation-agreements-ias/.

[3] Optical Internetworking Forum, "Implementation Agreement for Integrated Dual Polarization Micro-Intradyne Coherent Receivers," document OIF-DPC-MRX-02.0 (Jun. 2017), [Online] www.oiforum.com/technical-work/implementation-agreements-ias/.

[4] P.B. Zhang, C. Malouin, T.J. Schmidt, Towards full band colorless reception with coherent balanced receivers, Opt. Exp. 20 (9) (2012) 10339–10352, https://doi.org/10.1364/OE.20.010339.

[5] P.J. Reyes-Iglesias, A. Ortega-Moñux, I. Molina-Fernández, Calibrated Monolithically integrated 90° downconverter for colorless operation in the C+L band, IEEE Photon. J. 7 (2) (2015) 1–10, https://doi.org/10.1109/JPHOT.2015.2409091.

[6] D. Izquierdo, J. Clemente, P.J. Reyes-Iglesias, A. Ortega-Moñux, J.A. Altabás, I. Molina-Fernández, G. Wangüemert-Pérez, J. de Oliva-Rubio, I. Garcés, Analysis of the colorless operation of a calibrated 120° coherent receiver, J. Lightw. Technol. 39 (17) (2021) 5405–5411, https://doi.org/10.1109/JLT.2021.3069393.

[7] R. Matsumoto, et al., Scalable and Fast Optical Circuit Switch Based on Colorless Coherent Detection: Design Principle and Experimental Demonstration, J. Lightwave Technol. 39 (8) (2021) 2263–2274, https://doi.org/10.1109/JLT.2021.3050734.

[8] Y. Ma, L. Stewart, J. Armstrong, I.G. Clarke, G. Baxter, Recent progress of wavelength selective switch, J. Lightw. Technol. 39 (4) (2021) 896–903, https://doi.org/10.1109/JLT.2020.3022375.

[9] D. Lavery, et al., Opportunities for optical access network transceivers beyond OOK [invited], J. Opt. Commun. Networking 11 (2) (2019) A186–A195, https://doi.org/10.1364/JOCN.11.00A186.

[10] J. Zhang, G. Li, S. Xing, N. Chi, Flexible and adaptive coherent PON for next-generation optical access network [Invited], Opt. Fiber Technol. 75 (2023), https://doi.org/10.1016/j.yofte.2022.103190.

[11] M. Nooruzzaman, N. Alloune, C. Tremblay, P. Littlewood, M.P. Bélanger, Resource Savings in Submarine Networks Using Agility of Filterless Architectures, IEEE

Commun. Letters 21 (3) (2017) 512–515, https://doi.org/10.1109/LCOMM.2016.2634532.
[12] J. Kundrat, O. Havlis, J. Radil, J. Jedlinsky, J. Vojtech, Opening up ROADMs: a filterless add/drop module for coherent-detection signals, J. Opt. Commun. Netw. 12 (6) (2020) C41–C49, https://doi.org/10.1364/JOCN.388893.
[13] O. Ayoub, O. Karandin, M. Ibrahimi, A. Castoldi, F. Musumeci, M. Tornatore, Tutorial on filterless optical networks [Invited], J. Opt. Commun. Netw. 14 (3) (2022) 1–15, https://doi.org/10.1364/JOCN.437418.
[14] S. Gringeri, B. Basch, V. Shukla, R. Egorov, T.J. Xia, Flexible architectures for optical transport nodes and networks, IEEE Commun. Magazine 48 (7) (2010) 40–50, https://doi.org/10.1109/MCOM.2010.5496877.
[15] R. Kunkel, H.-G. Bach, D. Hoffmann, C.M. Weinert, I. Molina-Fernandez, R. Halir, First monolithic InP based 90 degrees-hybrid OEIC comprising balanced detectors for 100GE coherent frontends, IEEE Int. Conf. IPRM (2009) 167–170, https://doi.org/10.1109/ICIPRM.2009.5012469.
[16] M. Morsy-Osman, M. Chagnon, X. Xu, Q. Zhuge, M. Poulin, Y. Painchaud, M. Pelletier, C. Paquet, D.V. Plant, Analytical and experimental performance evaluation of an integrated Si-photonic balanced coherent receiver in a colorless scenario, Opt. Exp. 22 (5) (2014) 5693–5730, https://doi.org/10.1364/OE.22.005693.
[17] L.E. Nelson, X. Zhou, R. Isaac, Y. Lin, J. Chon, W.I. Way, Colorless reception of a single 100Gb/s channel from 80 coincident channels via an intradyne coherent receiver, IEEE Photon. Conf. (2012) 240–241, https://doi.org/10.1109/IPCon.2012.6358581.
[18] L.E. Nelson, S.L. Woodward, S. Foo, M. Moyer, D.J.S. Beckett, M. O'Sullivan, P. D. Magill, Detection of a single 40 Gb/s polarization multiplexed QPSK channel with a real-time intradyne receiver in the presence of multiple coincident WDM Channels, J. Lightw. Technol. 28 (20) (2010) 2933–2943, https://doi.org/10.1109/JLT.2010.2071853.
[19] I. Fatadin, S.J. Savory, D. Ives, Compensation of quadrature imbalance in an optical QPSK coherent receiver, IEEE Photon. Technol. Lett. 20 (20) (2008) 1733–1735, https://doi.org/10.1109/LPT.2008.2004630.
[20] S.J. Savory, Digital filters for coherent optical receivers, Opt. Exp. 16 (2) (2008) 804–817, https://doi.org/10.1364/OE.16.000804.
[21] M.S. Faruk, S.J. Savory, Digital signal processing for coherent transceivers employing multilevel formats, J. Lightwave Technol. 35 (5) (2017) 1125–1141, https://doi.org/10.1109/JLT.2017.2662319.
[22] P.J. Reyes-Iglesias, I. Molina-Fernández, A. Ortega-Moñux, Sensitivity penalty induced by non-ideal dual polarization downconverter in digital coherent receivers, Opt. Exp. 23 (10) (2015) 12784–12794, https://doi.org/10.1364/OE.23.012784.
[23] T. Pfau, S. Hoffmann, R. Noe, Hardware-efficient coherent digital receiver concept with feedforward carrier recovery for M -QAM constellations, J. Lightw. Technol. 27 (8) (2009) 989–999, https://doi.org/10.1109/JLT.2008.2010511.
[24] P.J. Reyes-Iglesias, I. Molina-Fernández, A. Moscoso-Mártir, A. Ortega-Moñux, High-performance monolithically integrated 120° downconverter with relaxed hardware constraints, Opt. Exp. 20 (5) (2012) 5725–5741, https://doi.org/10.1364/OE.20.005725.
[25] ITU-T Recommendation G.975.1: Forward error correction for high bit-rate DWDM submarine systems (02/2004).
[26] MACOM Corporate, Transimpedance amplifiers, [Online] https://www.macom.com/products/optical/-transimpedance-amplifier.
[27] P. Runge, et al., Monolithic InP receiver chip with a variable optical attenuator for colorless WDM detection, IEEE Photon. Technol. Lett. 26 (4) (2014) 349–351, https://doi.org/10.1109/LPT.2013.2293635.
[28] B. Zhang, C. Malouin, T.J. Schmidt, Design of coherent receiver optical front end for unamplified applications, Opt. Exp. 20 (3) (2012) 3225–3234, https://doi.org/10.1364/OE.20.003225.